



Society of Petroleum Engineers

SPE-200527-MS

Evaluating the Effects of Acid Fracture Etching Patterns on Conductivity Estimation Using Machine Learning Techniques

Mahmoud Desouky and Murtada Saleh Aljawad, King Fahd University of Petroleum and Minerals; Hamed Alhoori, Northern Illinois University; Dhafer Al-Shehri, King Fahd University of Petroleum and Minerals

Copyright 2020, Society of Petroleum Engineers

This paper was prepared for presentation at the SPE Europec featured at 82nd EAGE Conference and Exhibition originally scheduled to be held in Amsterdam, The Netherlands, 8 - 11 June 2020. Due to COVID-19 the physical event was postponed until 8 – 11 December 2020. The official proceedings were published online on 8 June 2020.

This paper was selected for presentation by an SPE program committee following review of information contained in an abstract submitted by the author(s). Contents of the paper have not been reviewed by the Society of Petroleum Engineers and are subject to correction by the author(s). The material does not necessarily reflect any position of the Society of Petroleum Engineers, its officers, or members. Electronic reproduction, distribution, or storage of any part of this paper without the written consent of the Society of Petroleum Engineers is prohibited. Permission to reproduce in print is restricted to an abstract of not more than 300 words; illustrations may not be copied. The abstract must contain conspicuous acknowledgment of SPE copyright.

Abstract

The successful design of an acid fracture job requires accurate prediction of fractured well productivity. Productivity estimation demands knowledge of both the acid penetration length and conductivity distribution for the given reservoir. The literature includes several models developed to predict the conductivity of acid fractured rock. The most popular is empirical and based on measuring the conductivity of 25 acid fracture experiments. The present research provides empirical models utilizing machine learning techniques and incorporating 97 experiments and 563 datapoints.

We conducted an extensive literature review to collect the published data on acid fracture experiments. The objective of such experiments is to measure conductivity at different formation closure stresses while considering field conditions. We used several data preprocessing techniques to clean the data, fill in missing values, exclude outliers and failed experiments, and standardize the dataset. Regularization was employed to eliminate features that didn't contribute to accurate prediction. Feature engineering was used to construct new features from our dataset. We began by measuring the correlations between features to better understand the data. We then built various machine learning models to predict acid fracture conductivity.

It has been observed that developing one universal empirical correlation often results in significant errors in conductivity estimation because different rock types result in different etching patterns that cannot be explained by a single correlation. For instance, the channeling etching pattern is mostly observed in limestone formations, while a roughness pattern is seen in dolomite and chalk rock. Moreover, the conductivities of etching patterns formed in chalk, dolomite, and limestone formations behave differently. We built machine learning classification techniques to determine the most likely etching patterns (e.g., channeling, roughness). A linear regression-based model was then developed as a baseline for comparison with other models generated through ridge regression. We evaluated the performances of our models using well-known metrics such as accuracy, precision, recall, mean squared error, and correlation coefficients. We also employed cross-validation to avoid over-fitting, finding that certain features were the most important in predicting acid fracture conductivity.

Detailed empirical conductivity correlations and models were developed in this work for three carbonate rock types. Previously, a single empirical model has often been employed to estimate acid fracture conductivity or, at best, a model has been developed for a particular rock type. Most models have not considered the impact of etching patterns on conductivity, which was found to be significant in limestone.

Introduction

Acid fracturing is a well stimulation method applied to tight carbonate reservoirs. A hydraulic fracture is created when the treatment pressure exceeds the formation breakdown pressure. The formation stresses usually close the hydraulic fracture once pumping ceases. Prior to this cessation, fracture face asperities prop the fracture open against closure stress, providing a conductive path for reservoir fluids. Rock heterogeneity results in uneven surfaces, improving fracture conductivity (Williams et al., 1979; Asadollahpour et al., 2018). Conductivity is defined as the ability of a fracture to deliver fluids; it decreases as the formation closure stress increases. A successful acid fracture job produces sufficient durable conductivity.

Predicting acid fracture conductivity is essential to improving acid fracture design. Acid/rock dissolution is a stochastic phenomenon that depends on a number of parameters. Thus, prediction of the resulting conductivity can be challenging. Different approaches have been taken to predict acid fracture conductivity, as summarized in Table 1. Empirical correlations based on experimental studies are convenient to apply because their parameters are easy to obtain. Analytical correlations based on theoretical derivations are complicated and require sophisticated parameters. These parameters may demand experiments to tune them for a regression analysis. Artificial intelligence models require accurate, consistent, and sizeable datasets to be viable.

Table 1—Conductivity Correlations

Analytical	Numerical	Empirical	Artificial Intelligence
Gangi, 1978	Deng-Mou et al., 2010	Nierode-Kruck, 1973	Akbari et al., 2017
Walsh, 1981	Kamali et al., 2015	Nasr-Eldin et al., 2006	Eliebid et al., 2018
Gong, 1997		Pournik, 2009	Motamedi-Ghahfarokhi et al., 2018

Nierode and Kruck (1973) suggested that among other parameters, the amount of rock dissolved can be used to determine acid fracture conductivity. Recent research has also shown that the pattern of rock removal has a crucial effect on hydraulic fracture conductivity, even more so than the amount of dissolved rock (Pournik, 2008). For instance, conductivity is higher when the acid fracture treatment generates channels instead of rough surfaces, given that such channels withstand closure stress (van Domelen et al., 1994; Ruffet et al., 1998; Beg et al., 1998; Nieto et al., 2006; Melendez, 2007; Antelo, 2009; Cash, 2016; Kamali et al., 2016; Lu et al., 2017). The leak-off of acid into the formation matrix can also result in more heterogeneous fracture surfaces that boost conductivity when the rock's mechanical properties are unharmed (Beg et al., 1998).

Pournik (2008) categorized etching patterns of rock samples after acidization into five categories. The roughness etching pattern occurs when acid etches the rock, leaving asperities distributed on the fracture surface. The channeling etching pattern is characterized by a V-shape where the acid etches the middle more than the edges. Cavity and turbulence etching patterns are similar in that pockets are formed by the acid etching. The uniform etching pattern occurs due to low reactivity of the rock with the acid or rock mineral homogeneity. In similar acid systems, contact time can influence the etching pattern. Also, acid concentration, which changes along the fracture length, affects the amount of rock dissolved as well as the etching pattern (Pournik et al., 2013). Roughness is more likely to be generated when smooth surfaces are being acidized, while acidization of rough surfaces deepens valleys and smoothens peaks (Al-Momin

et al., 2014). Pournik (2008) employed both theoretical and empirical methods to develop conductivity correlations for the roughness etching pattern, considering each rock type separately.

Few models account for the contribution of channels to conductivity, which provide higher conductivity at low stress and durable conductivity after fracture closure. Large channel dimensions make the flow easier and pressure drop lower. Deng and Mou (2012) captured their effect through numerical studies, enhancing conductivity prediction. They classified etching patterns into three categories: permeability distribution dominant, mineralogy distribution dominant, and competing effect of permeability and mineralogy distributions. To apply their correlations, six parameters are needed: ideal fracture width, ideal Young's modulus, calcite fraction, horizontal and vertical correlation lengths, and standard deviation for permeability distribution. Almomen (2013) showed that rough surface fractures generate conductivity an order of magnitude higher than do smooth surface fractures at low closure stresses. Thus, ignoring such factors will yield simple models, but such models will be inaccurate and biased. We investigated the effects of different features such as etching patterns on conductivity prediction.

Data Gathering and Handling

An extensive literature review was conducted to collect published data on acid fracture experiments (Hill et al., 2007; Melendez, 2007; Pournik, 2009; Almomen, 2013; Nino, 2013; Cash, 2016; Jin et al., 2019). The physical properties, meanings, and units of different features are described in Table 2.

Table 2—Physical Meaning of Features

Feature	Symbol	Physical Meaning and Unit
Rock Type	X^1	Rocks etched by different acids
Acid Type	X^2	Acid systems used to etch rocks
Rock Surface	X^3	Initial rock surface before acid etching
Etching Pattern	X^4	Manner of rock surface behavior after acid etching
Temperature	X^5	Temperature of etching acid in °F
Injection Rate	X^6	Rate of pumping acid through API conductivity cell in liters per minute
Injection Time	X^7	Time for pumping acid through API conductivity cell in minutes
Acid Concentration	X^8	Concentration of etching acid pumped through API conductivity cell as a percentage
Stress	X^9	Applied stress by loading frame in psi
Conductivity	Y	Resultant rock conductivity under stress in md-ft

The objective of the acid fracture experiment was to measure conductivity at different formation closure stresses while mimicking field conditions (e.g., rock type, acid type, injection rate, treatment volume). The conditions were scaled down to represent the field conditions. The rock types and their initial surface conditions were tabulated, along with the treatment conditions (e.g., temperature, injection time). Next, the etching pattern and conductivity at each load stress were compiled to complete the dataset, as shown in Table 3 (Desouky, 2019). Therefore, the data gathered were consistent because the datapoints came from the same modified API RP-61 conductivity cell (Zou, 2006).

Table 3—Sample of Data Collected

X^1	X^2	X^3	X^4	X^5	X^6	X^7	X^8	X^9	Y
Chalk	GelledAcid	Rough	Channeling	175	1	30	15	3000	90
Chalk	Straight	Smooth	Turbulence	175	1	5	15	100	2778

X^1	X^2	X^3	X^4	X^5	X^6	X^7	X^8	X^9	Y
Dolomite	GelledAcid	Smooth	Rough	130	0.5	20	15	500	127
Dolomite	GelledAcid	Smooth	Rough	130	0.5	20	15	1000	104
Limestone	GelledAcid	Rough	Rough	175	1	30	15	5000	72
Limestone	Emulsified	Smooth	Rough	200	1	15	15	1000	1597

Outliers and failed experiments were excluded to obtain the data most appropriate for building the model. Table 4 includes a statistical summary of the different numerical features.

Table 4—Statistical Summary of Numerical Features

	X^5	X^6	X^7	X^8	X^9	Y
Mean	162.7	1.0	19.0	16.0	2,764.1	2,534.7
Median	175.0	1.0	15.0	15.0	3,000.0	366.0
Mode	175.0	1.0	10.0	15.0	1,000.0	72.0
Standard Deviation	36.2	0.1	12.9	3.0	1768.8	7,048.3
Variance	1,309.0	0.0	165.7	8.9	3,128,639.2	49,678,784.6
Range	175.0	0.5	55.0	13.0	7,500.0	72,483.0
Minimum	100.0	0.5	5.0	15.0	0.0	0.0
Maximum	275.0	1.0	60.0	28.0	7,500.0	72,483.0

There were different types of predictors and features among the gathered data, both categorical and numerical. The ranges of numerical features differed. For instance, temperature ranged from 100°F to 275°F, and stress from 0 to 7,500 psi. The stress range was roughly 43 times greater than the temperature range. Thus, these two features were very different. When further analyses were conducted (e.g., multivariate linear regression), the attributed stress intrinsically influenced the result to a greater extent, due to its larger value. However, this did not necessarily mean it was more important as a predictor. The predictors considered were $\{X^1, X^2, \dots, X^n\}$, where the superscript j is an index ranging from 1 to the total number of predictors n . Each predictor X contained m datapoints, x_i^j , where the subscript i is an index ranging from 1 to the total number of points m . The goal of normalization was to alter these features in the dataset to reside on a common scale without changing the difference in the value range. Therefore, prior to modelling, the normalization of the numerical features was accomplished by subtracting their means and scaling them to unit variance, as per Equation (1):

$$z_i^j = \frac{x_i^j - \mu^j}{\sigma^j} \quad (1)$$

where z_i^j is the z-score or normalized value of each data point, μ^j is the mean value of each predictor X , and σ^j is the standard deviation of the predictor.

Method

There were two goals for this research (see Figure 1). The first was to classify the etching patterns based on rock type and treatment condition. A multi-class algorithm was needed to label the different classes, depending on various conditions. The second goal was predicting the conductivity of the different rock

types, using the most relevant features. Multi-variant regression was a simple and robust approach to obtaining a predictive model.

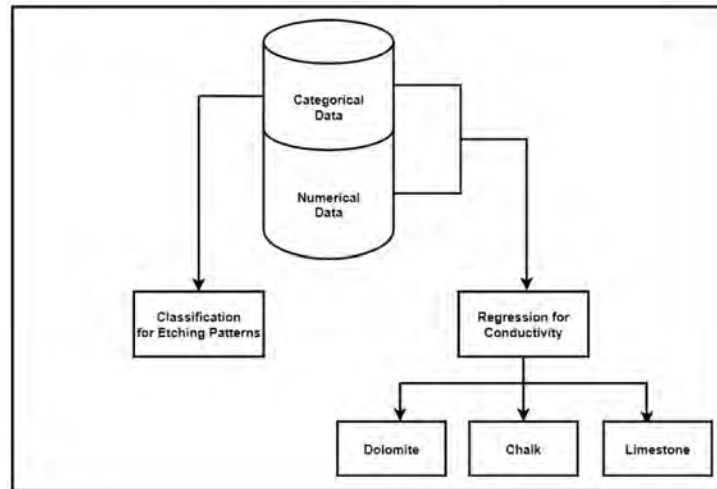


Figure 1—Models Targeted and Data Used

Classification of Etching Patterns

Ensemble templates can be employed to train multiclass error-correcting output codes models. The template employed here had three arguments: method, number of learners, and learner. We specified in the following way. The method was "GentleBoost," the number of learners was 100, and the learner was a decision tree. As a classifier, the decision tree splits data based on various conditions. Multi-classification is similar to binary classification, but with a minor modification. One class is regarded as positive and the rest are negative. Ensemble learning is an aggregation of multiple options that decreases the possibility of choosing a poor model.

Regression for conductivity prediction

The essence of regression as used in the present research is to reduce the cost function $J(\vec{\theta})$ through gradient descent. The cost function is a measure of how wrong the model is when estimating the responses from predictors. A gradient descent minimizes the cost function by finding the weights, θ_j , that make $\frac{\partial}{\partial \theta_j} J(\vec{\theta})$ equal to zero. The hypothesis h_θ differentiates between linear and non-linear regressions. Directly using the feature values means a linear hypothesis, whereas introducing a logarithm or power to the feature values makes the hypothesis non-linear. The hypothesis function is sensitive to slight changes in the coefficients. The coefficients' values change by a significant amount as the training data change. Thus, regularized linear regression was appropriate for this problem. Regularization is used to drop features that do not contribute to a good prediction. The regularization term has different forms and the regression is named based on whether it is ridge, lasso, or elastic net. Fitting a linear regression model to data can result in coefficients with large variances. Regularization reduces the variance of the coefficients, yielding models with smaller prediction errors. Here, ridge regression was used, and the cost function is defined as in Equation (2):

$$J(\vec{\theta}) = \frac{1}{2m} \sum_{i=1}^m (h_\theta(x^{(i)}) - y^{(i)})^2 + \lambda \sum_{j=1}^n \theta_j^2 \quad (2)$$

where $J(\vec{\theta})$ is the cost function, m is the number of datapoints, $y^{(i)}$ is the actual response at the datapoint i , λ is the regularization parameter, n the number of predictors, θ_j is the weight multiplied by the feature j ,

and $h_{\theta}(x^{(i)})$ is the hypothesis. The hypothesis consisted of a combination of X s multiplied by θ s, depending on the design matrix.

Results and Discussion

Classification of Etching Patterns

Rock surface, acid type, and rock type were used as predictors for 80% of the data (78 experiments) in order to train the model with five-fold cross-validation. The last 20% of the data (19 experiments) was used to test the classifier. The classifier had a test error of .0833. The overall accuracy was 94.7%. All precision and recall values are summarized in Figure 2. The corner square to the right of the figure shows the overall accuracy of the classifier. The rows are relevant to the predicted class, while columns are to the actual class. The diagonal squares indicate the observations that were correctly classified. The off-diagonal squares are incorrectly classified observations. The number of observations and their percentages are shown in each square. The rightmost column includes the percentages of all observations predicted to belong to each class that were correctly or incorrectly classified. This metric is called precision. The bottom row includes the percentages of all observations belonging to each class that were correctly or incorrectly classified. This metric is called the true positive rate (i.e., recall).

Predicted Class	Channeling	2 10.5%	0 0.0%	0 0.0%	0 0.0%	100% 0.0%
	Roughness	0 0.0%	13 68.4%	0 0.0%	0 0.0%	100% 0.0%
	Turbulence	0 0.0%	0 0.0%	2 10.5%	0 0.0%	100% 0.0%
	Uniform	1 5.3%	0 0.0%	0 0.0%	1 5.3%	50.0% 50.0%
		66.7% 33.3%	100% 0.0%	100% 0.0%	100% 0.0%	94.7% 5.3%
	Channeling	Roughness	Turbulence	Uniform	Actual Class	

Figure 2—Confusion matrix of the etching pattern classifier.

Precision and recall become more important when the data are skewed or unbalanced. For instance, the dolomite generated a roughness etching pattern in 90.6% of the experiments. There was an unbalance in the etching pattern generated. If an etching pattern classifier for dolomite only was set to always output roughness, the overall accuracy would be higher than 90%. Any other etching pattern would be misclassified. Thus, assessment of a classifier based on overall accuracy alone when there is a severe class imbalance is inaccurate.

Regression for conductivity prediction

Dolomite. Data often contain predictors that do not have any relationship with the response. These predictors should not be included in the model. It is better to have a limited number of predictors, yet hold nearly complete variance of the data (Kazakov et al., 2011). One way to select the most relevant predictors for response is to repeatedly train the model while adding predictors and monitoring loss. At a specific point, adding more predictors will not increase the accuracy, only calculation time and memory consumption.

The acid type, rock surface, and etching pattern were transformed into dummy variables to make the entire dataset homogeneous as numeric values. For instance, a categorical predictor that contained a number of categories equal to K was transformed into K-1 predictors of zeros and ones.

Figure 3 shows the minimum number of predictors sufficient to obtain the least loss in the multivariate linear model for predicting the conductivity of dolomite. Adding the temperature and etching pattern significantly decreased loss. The loss then remained the same after adding rock surface and acid type.

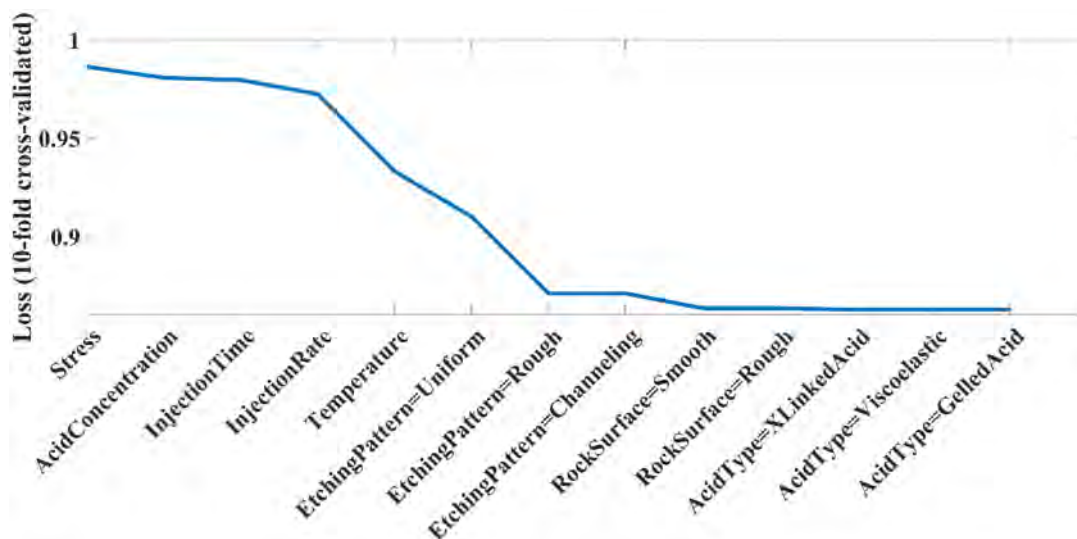


Figure 3—Lowest number of predictors to obtain the least loss for dolomite.

The predictors that resulted in the least loss in Figure 3 were used to obtain the first dolomite model. The predictors beginning with "Stress" and ending with "RockSurface=Roughness" were selected. The design matrix was built using the MATLAB software function "x2fx." One of the following four models needed to be specified first: "linear," "interactions," "quadratic," or "purequadratic." The ten-predictor matrix was converted to a design matrix using the "quadratic" model. The learning curve in Figure 4 shows high variance that cannot be addressed by regularization or simplification of the model. This means that more data were needed. The correlation coefficient between the fitted and actual values was 94.9%, and the normalized MSE was 0.03. This model contained 52 parameters and could not have been easily implemented. Thus, other models were trained with different combinations of predictors to obtain a simpler model with fair performance. A simpler model was obtained using the first four predictors, starting with "Stress" and ending with "InjectionRate." The bias and weights are summarized in Table 5.

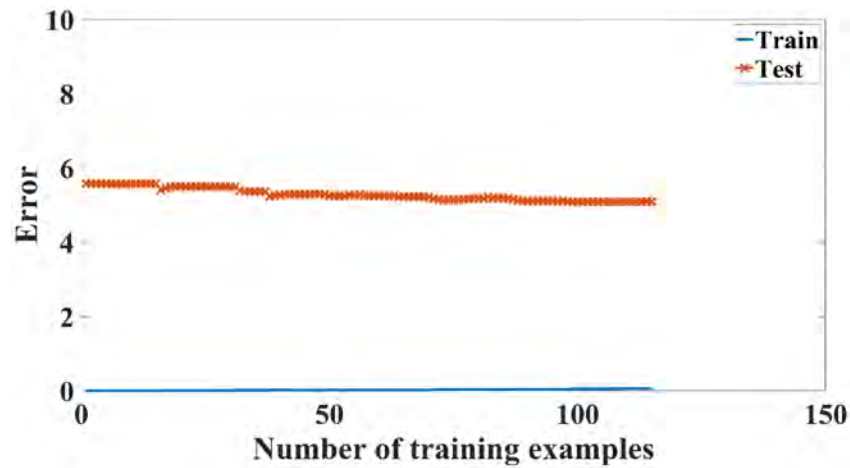


Figure 4—Learning curve for dolomite.

Table 5—Detailed Conductivity Model for Dolomite

Parameter	Value
Bias	0.7969
X^6	0.1103
X^7	0.5616
X^8	-0.0107
X^9	-0.2002
$X^6 * X^7$	0.3348
$X^6 * X^8$	-0.0325
$X^6 * X^9$	-0.0738
$X^7 * X^8$	-0.1305
$X^7 * X^9$	-0.0548
$X^8 * X^9$	0.0145
$(X^6)^2$	-0.1686
$(X^7)^2$	-0.6016
$(X^8)^2$	-0.0402
$(X^9)^2$	0.0309

The values predicted for dolomite conductivity were plotted against the actual ones, as shown in Figure 5. The fitted values at high stresses were less than the actual values, which was as expected.

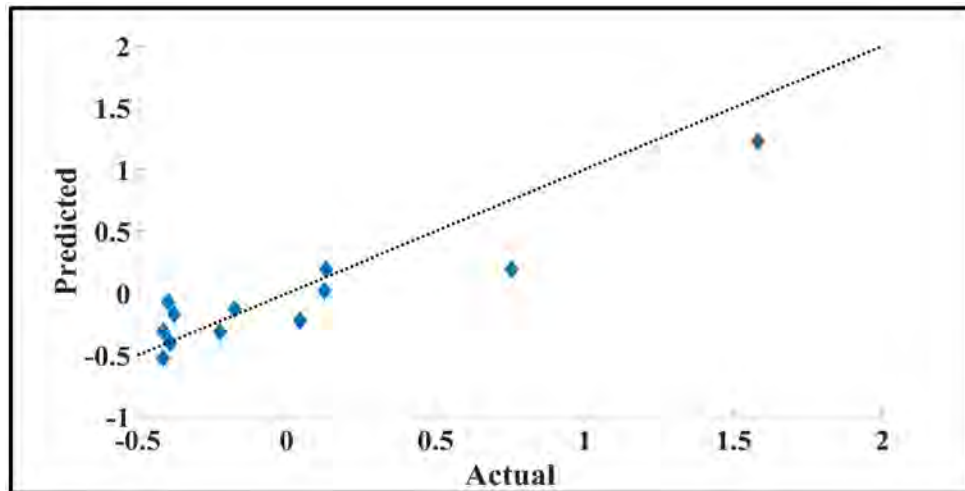


Figure 5—Actual vs. predicted values of dolomite.

The correlation coefficient between the fitted and actual values was 93.1%, and the normalized MSE was 0.05. The error distribution was slightly asymmetric, as shown in Figure 6.

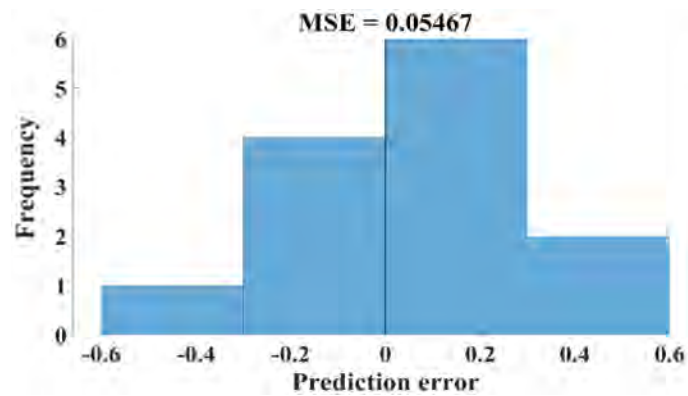


Figure 6—Error distribution of the dolomite conductivity predictions.

Chalk. Figure 7 shows the minimum number of predictors sufficient to obtain the lowest loss in the multivariate linear model for predicting the conductivity of chalk. Thus, "Stress," "InjectionTime," "Temperature," and "EtchingPattern=Turbulence" were selected as predictors. The chalk conductivity model was created by training a polynomial regression model of the four predictors selected, their quadratic values, and their interactions with one another.

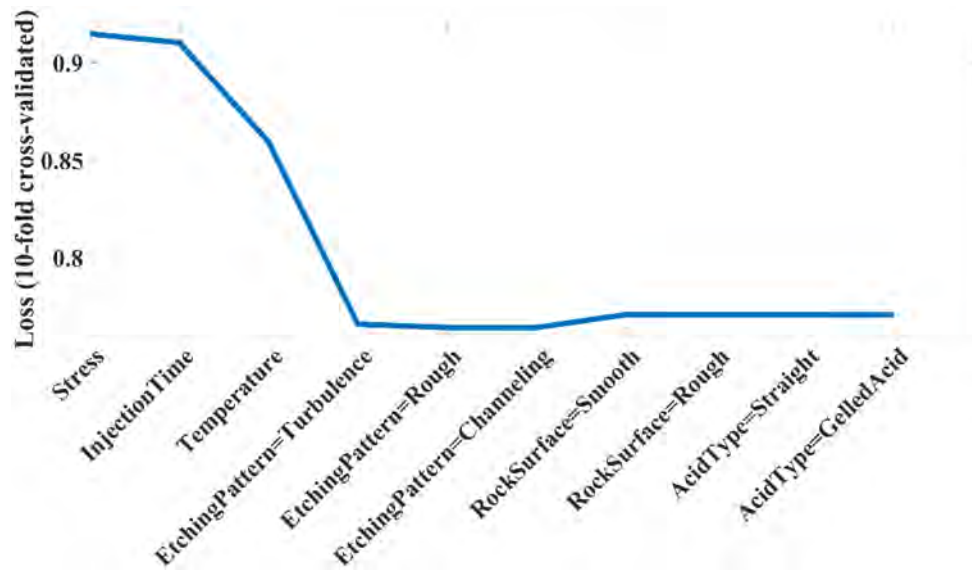


Figure 7—Lowest number of predictors yielding the least loss for chalk.

The learning curve in Figure 8 shows a good fit, as the two curves plateau at a low error value. The regularization parameter selected was 0.001 because the cross-validation error was at a minimum at this value.

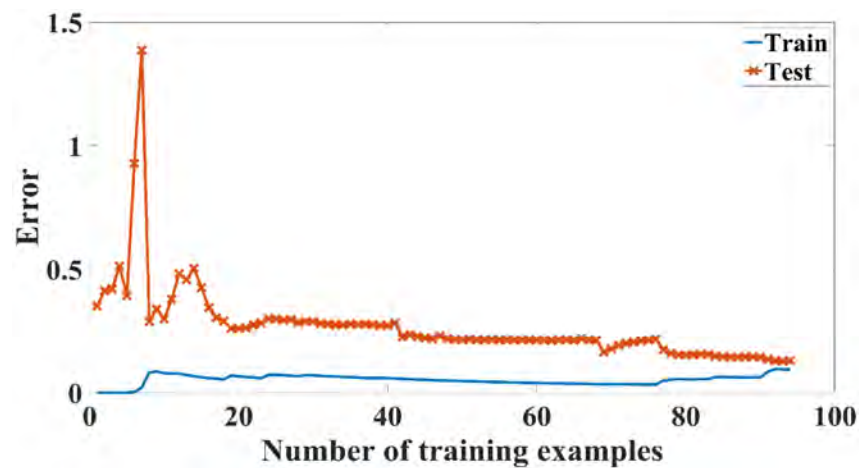


Figure 8—Learning curve for chalk.

The values predicted for chalk conductivity were then plotted against the actual ones (see Figure 9).

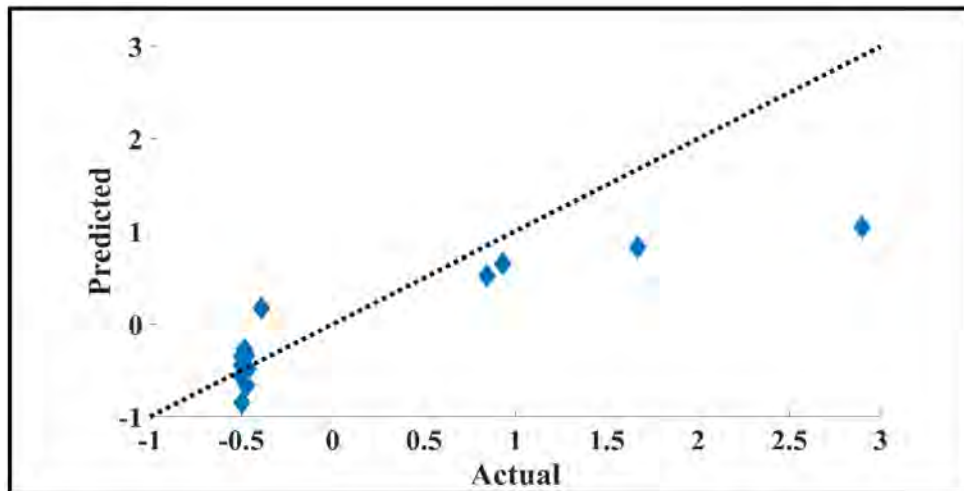


Figure 9—Actual vs Predicted on 45-Degree line of Chalk

The correlation coefficient between the fitted and actual values was 90.6%. The error distribution for chalk conductivity indicates nearly symmetric behavior, as seen in Figure 10. Most of the errors were between [-1, 0] and [0, 1], with almost the same frequency.

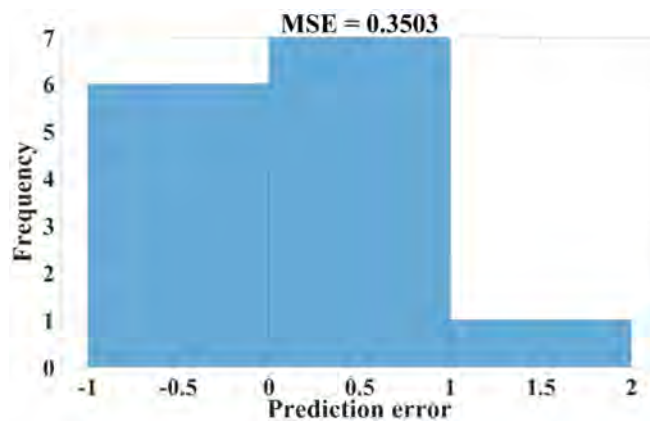


Figure 10—Error distribution of chalk.

For dolomite and chalk, it was possible to train simpler models with fewer predictors. This was because they often developed a roughness etching pattern (see Table 6). A simpler model for chalk conductivity with the same performance as the previous model appears in Table 7.

Table 6—Correlations between Etching Pattern and Rock Type

	Channeling	Rough	Turbulence	Uniform	Total
Dolomite	5	125	8	0	138
	3.6%	90.6%	5.8%	0%	100%
Chalk	6	100	11	0	117
	5.1%	85.5%	9.4%	0%	100%
Limestone	85	142	33	30	290
	29.3%	49%	11.4%	10.3%	100%

Table 7—Detailed Conductivity Model for Chalk

Parameter	Value
Bias	0.3769
X^5	-0.1179
X^7	0.2851
X^9	-0.3391
$X^5 * X^7$	-0.0672
$X^5 * X^9$	-0.0867
$X^7 * X^9$	0.0232
X^5^2	-0.5476
X^7^2	-0.0567
X^9^2	0.1459

Limestone. Predicting limestone conductivity can be problematic because the material generates all kinds of etching patterns. Thus, to develop a reasonable conductivity model, high conductivity values were expected first. A classifier was developed using ensemble classification based on the treatment and original surface conditions. The classifier's accuracy was 93% (see Figure 11). The output of this classifier was then fed into the polynomial regression model as an additional predictor.

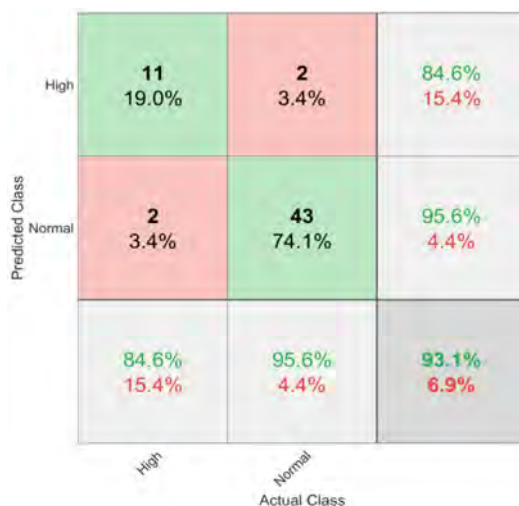


Figure 11—Confusion matrix of normal and high limestone conductivities.

The high conductivity values were labelled "Conductivity=High" and the normal values were labelled "Conductivity=Normal." The confusion matrix misclassified four high conductivity datapoints in the test dataset. Error analysis was performed to investigate why this misclassification occurred. The channels could be considered open slots, the conductivity of which depended on the width of the channel. Some channels were more conductive than others because they were wider. The V-shaped angle of the channel itself impacted its sustainability under stress. For instance, if the angle of the V-shape was acute, it collapsed at higher stresses than would an obtusely angled channel.

Figure 12 shows the minimum number of predictors sufficient to obtain the lowest loss in the multivariate linear model predicting the conductivity of limestone. Thus, the predictor "Stress" was selected for the beginning and "AcidType=Straight" for the end. The loss curve began to increase as the number of predictors grew, due to overfitting of the data by training.

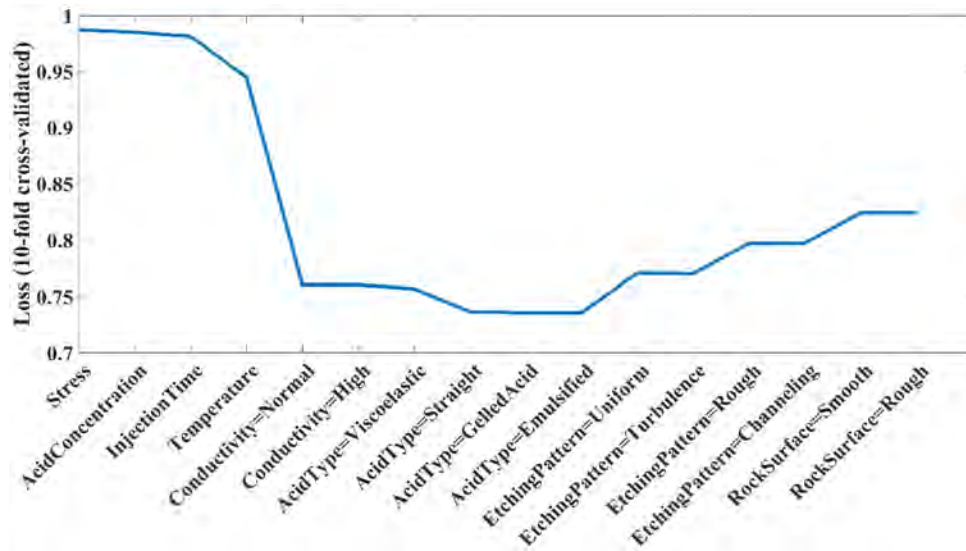


Figure 12—Lowest number of predictors to obtain the least loss for limestone.

Several limestone conductivity models were created by training a polynomial regression model with different combinations of predictors. The simplest is tabulated in Table 8. The learning curve in Figure 13 shows a slightly high variance as the training curve plateaus, whereas the test error had a higher value. The regularization parameter was selected to be 0.003 because the cross-validation error was at a minimum at this value.

Table 8—Detailed Conductivity Model for Limestone

Parameter	Value
Bias	0.2374
Conductivity=Normal	-0.5451
X^5	0.4974
X^9	-0.8598
Conductivity=Normal* X^5	-0.4680
Conductivity=Normal* X^9	0.7245
X^5*X^9	-0.1317
AcidType=Viscoelastic	-0.0700
AcidType=Straight	0.1103
$(X^9)^2$	-0.0008

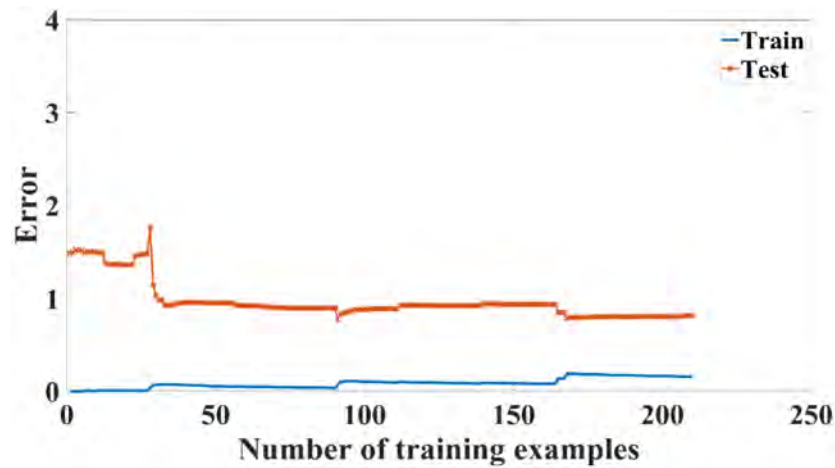


Figure 13—Learning curve for limestone.

The values predicted for chalk conductivity were then plotted against the actual ones (see Figure 14).

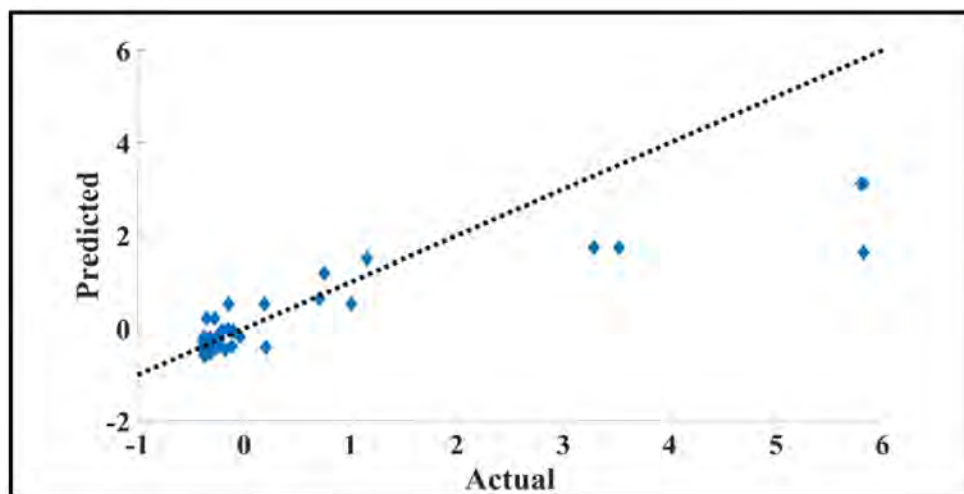


Figure 14—Actual vs. predicted values for limestone.

The correlation coefficient between the fitted and actual values was 91.9%. The error distribution of limestone conductivity was asymmetrical, as there were high conductivity points that could not be forecast by the model (see Figure 15). These extremely high conductivity values were not expected by the classifier or the conductivity model. The values were two to three orders of magnitude higher than the normal values. The overall error was amplified to 0.686, due to the presence of these points.

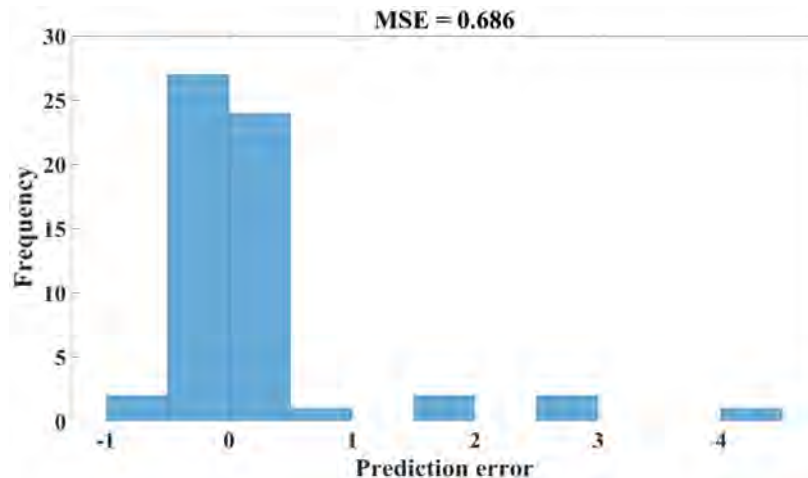


Figure 15—Error distribution of limestone.

Conclusion

The etching pattern that results from acid fracturing has a more significant impact on limestone acid fracture conductivity than on that of chalk and dolomite. Dolomite and chalk both developed a roughness etching pattern in more than 85% and 90% of the acid etching experiments, respectively. Limestone developed a roughness etching pattern in less than 50% and a channeling etching pattern in 30% of the acid etching experiments. Limestone's extremely high conductivity channels could not be fitted by the model and increased errors. Most errors in acid fracture conductivity estimation happen at low stresses when the fracture behaves like an open slot, or at high stresses when the rock fails unexpectedly under closure stress.

References

- Akbari, M., Javad Ameri, M., Kharazmi, S., Motamedi, Y., & Pournik, M. (2017). New correlations to predict fracture conductivity based on the rock strength. *Journal of Petroleum Science and Engineering*, **152**, 416–426.
- Aljawad, M. S., Aljulaih, H., Hughes, B., & Desouky, M. (2019). Integration of field, laboratory, and modeling aspects of acid fracturing: A comprehensive review. *Journal of Petroleum Science and Engineering*.
- Almomen, A. M. (2013). *The Effects of Initial Condition of Fracture Surfaces, Acid Spending, and Type on Conductivity of Acid Fracture* (Doctoral dissertation).
- Antelo, L. F., Zhu, D., & Hill, A. D. (2009, January). Surface characterization and its effect on fracture conductivity in acid fracturing. *In SPE Hydraulic Fracturing Technology Conference*. Society of Petroleum Engineers.
- Asadollahpour, E., Baghbanan, A., Hashemolhosseini, H., & Mohtarami, E. (2018). The etching and hydraulic conductivity of acidized rough fractures. *Journal of Petroleum Science and Engineering*, **166**, 704–717.
- Beg, M. S., Kunak, A. O., Gong, M., Zhu, D., & Hill, A. D. (1998). A Systematic Experimental Study of Acid Fracture Conductivity. *SPE Production & Facilities*, **13**(04), 267–271.
- Cash, R. J. (2016). *Acid fracturing carbonate-rich shale: a feasibility investigation of eagle ford formation* (Doctoral dissertation).
- Deng, J., Mou, J., Hill, A. D., & Zhu, D. (2012). A New Correlation of Acid-Fracture Conductivity Subject to Closure Stress. *SPE Production & Operations*, **27**(02), 158–169.
- Desouky, M. (2019). *Enhancement and Prediction of Long-Term Acid Fracture Conductivity* (Master thesis, King Fahd University of Petroleum and Minerals).
- Eliebid, M., Hassan, A. M., Mahmoud, M., Abdulraheem, A., & Elkatatny, S. (2018, August). Intelligent Prediction of Acid-Fracturing Performance in Carbonates Reservoirs. *In SPE Kingdom of Saudi Arabia Annual Technical Symposium and Exhibition*. Society of Petroleum Engineers.
- Hill, A. D., Pournik, M., Zou, C., Malagon Nieto, C., Melendez, M. G., Zhu, D., & Weng, X. (2007, January). Small-scale fracture conductivity created by modern acid fracture fluids. *In SPE Hydraulic Fracturing Technology Conference*. Society of Petroleum Engineers.
- Gangi, A. F. (1978, October). Variation of whole and fractured porous rock permeability with confining pressure. *In International Journal of Rock Mechanics and Mining Sciences & Geomechanics Abstracts* (Vol. **15**, No. 5, pp. 249–257). Pergamon.

- Gong, M. (1997). *Mechanical and hydraulic behavior of acid fractures: experimental studies and mathematical modeling* (Doctoral dissertation, University of Texas at Austin).
- Jin, X., Zhu, D., Hill, A. D., & McDuff, D. (2019, January 29). Effects of Heterogeneity in Mineralogy Distribution on Acid Fracturing Efficiency. Society of Petroleum Engineers. doi: [10.2118/194377-MS](https://doi.org/10.2118/194377-MS)
- Kamali, A., & Pournik, M. (2015, January). Rough Surface Closure—A Closer Look at Fracture Closure and Conductivity Decline. In *ISRM Regional Symposium-EUROCK 2015*. International Society for Rock Mechanics and Rock Engineering.
- Kamali, A., & Pournik, M. (2016). Fracture closure and conductivity decline modeling – Application in unproped and acid etched fractures. *Journal of Unconventional Oil and Gas Resources*, **14**, 44–55.
- Kazakov, N., & Miskimins, J. L. (2011, January). Application of multivariate statistical analysis to slickwater fracturing parameters in unconventional reservoir systems. In *SPE Hydraulic Fracturing Technology Conference*. Society of Petroleum Engineers.
- Lu, C., Bai, X., Luo, Y., & Guo, J. (2017). New study of etching patterns of acid-fracture surfaces and relevant conductivity. *Journal of Petroleum Science and Engineering*, **159**, 135–147.
- Melendez, M. G., Pournik, M., Zhu, D., & Hill, A. D. (2007, January). The effects of acid contact time and the resulting weakening of the rock surfaces on acid fracture conductivity. In *European Formation Damage Conference*. Society of Petroleum Engineers.
- Motamedi-Ghahfarokhi, Y., Ameri Shahrabi, M. J., Akbari, M., & Pournik, M. (2018). New correlations to predict fracture conductivity based on the formation lithology. *Energy Sources, Part A: Recovery, Utilization, and Environmental Effects*, **40**(13), 1663-1673.
- Nierode, D. E., & Kruk, K. F. (1973, January). An evaluation of acid fluid loss additives retarded acids, and acidized fracture conductivity. In *Fall Meeting of the Society of Petroleum Engineers of AIME*. Society of Petroleum Engineers.
- Nieto, C. M., Pournik, M., & Hill, A. D. (2008). The texture of acidized fracture surfaces: implications for acid fracture conductivity. *SPE Production & Operations*, **23**(03), 343-352.
- Nino Penaloza, A. (2013). *Experimental Study of Acid Fracture Conductivity of Austin Chalk Formation* (Doctoral dissertation).
- Pournik, M. (2008). *Laboratory-scale fracture conductivity created by acid etching*. Texas A&M University.
- Pournik, M., Zhu, D., & Hill, A. D. (2009, January). Acid-fracture conductivity correlation development based on acid-etched fracture characterization. In *8th European Formation Damage Conference*. Society of Petroleum Engineers.
- Pournik, M., Gomma, A. M., & Nasr-El-Din, H. A. (2010, January). Influence of acid-fracture fluid properties on acid-etched surfaces and resulting fracture conductivity. In *SPE International Symposium and Exhibition on Formation Damage Control*. Society of Petroleum Engineers.
- Pournik, M., Li, L., Smith, B. T., & Nasr-El-Din, H. A. (2013). Effect of acid spending on etching and acid-fracture conductivity. *SPE Production & Operations*, **28**(01), 46-54.
- Ruffet, C., Fery, J. J., & Onaisi, A. (1998). Acid Fracturing Treatment: a Surface Topography Analysis of Acid Etched Fractures to Determine Residual Conductivity. *SPE Journal*, **3**(02), 155–162.
- Van Domelen, M. S., Gdanski, R. D., & Finley, D. B. (1994, January). The application of core and well testing to fracture acidizing treatment design: a case study. In *European Production Operations Conference and Exhibition*. Society of Petroleum Engineers.
- Walsh, J. B. (1981, October). Effect of pore pressure and confining pressure on fracture permeability. In *International Journal of Rock Mechanics and Mining Sciences & Geomechanics Abstracts* (Vol. **18**, No. 5, pp. 429-435). Pergamon.
- Williams, B. B., Gidley, J. L., & Schechter, R. S. (1979). Acidizing Fundamentals, *Henry L. Doherty Memorial Fund of AIME*, Society of Petroleum Engineers of AIME, New York.
- Zou, C. (2006). Development and Testing of an Advanced Acid Fracture Conductivity Apparatus. 2006. 59 f. Master of Science Thesis-Texas A&M University.